Nanoscale

PAPER

Self-assembly of a robust hydrogen-bonded octylphosphonate network on cesium lead bromide perovskite nanocrystals for light-emitting diodes†

Cite this: DOI: 10.1039/c9nr02566a

Alasdair A. M. Brown, *[a,b,c,d] Thomas J. N. Hooper,[d] Sjoerd A. Veldhuis,[d] Xin Yu Chin,[d] Annalisa Bruno,[d] Parth Vashishtha,[d,e] Ju Nie Tey,[b] Liudi Jiang,[a] Bahulayan Damodaran,[d] Suan Hui Pu,[a,c] Subodh G. Mhaisalkar[d,e] and Nripan Mathews *[d,e]

We report the self-assembly of an extensive inter-ligand hydrogen-bonding network of octylphosphonates on the surface of cesium lead bromide nanocrystals ($CsPbBr_3$ NCs). The post-synthetic addition of octylphosphonic acid to oleic acid/oleylamine-capped $CsPbBr_3$ NCs promoted the attachment of octylphosphonate to the NC surface, while the remaining oleylammonium ligands maintained the high dispersability of the NCs in non-polar solvent. Through powerful 2D solid-state ^{31}P–^{1}H NMR, we demonstrated that an ethyl acetate/acetonitrile purification regime was crucial for initiating the self-assembly of extensive octylphosphonate chains. Octylphosphonate ligands were found to preferentially bind in a monodentate mode through P–O^-, leaving polar P═O and P–OH groups free to form inter-ligand hydrogen bonds. The octylphosphonate ligand network strongly passivated the nanocrystal surface, yielding a fully-purified $CsPbBr_3$ NC ink with PLQY of 62%, over 3 times higher than untreated NCs. We translated this to LED devices, achieving maximum external quantum efficiency and luminance of 7.74% and 1022 cd m^{-2} with OPA treatment, as opposed to 3.59% and 229 cd m^{-2} for untreated $CsPbBr_3$ NCs. This represents one of the highest efficiency LEDs obtained for all-inorganic $CsPbBr_3$ NCs, accomplished through simple, effective passivation and purification processes. The robust binding of octylphosphonates to the perovskite lattice, and specifically their ability to interlink through hydrogen bonding, offers an promising passivation approach which could potentially be beneficial across a breadth of halide perovskite optoelectronic applications.

Received 25th March 2019,
Accepted 31st May 2019

DOI: 10.1039/c9nr02566a

rsc.li/nanoscale

Introduction

Lead halide perovskite nanocrystals (NCs) have recently demonstrated exceptional promise as emissive materials for light-emitting diodes (LEDs).[1–3] They present combined advantages including low-temperature, cost-effective solution-processing techniques and outstanding optoelectronic properties. These halide perovskites have demonstrated high photoluminescence quantum yields (PLQYs) across the full visible range, owing to their compositional versatility, with narrow emission bands (FWHM < 20 nm).[4–7]

Compared to other emissive nanomaterials, such as metal chalcogenides, nanocrystals (NCs) of halide perovskites are particularly suitable for light-emission,[8] owing to their much higher defect tolerance.[9] For example, vacancies only manifest as shallow trap states in the perovskite lattice,[10] therefore NCs with high photoluminescence quantum yield (PLQY) can be achieved from straight-forward low-temperature chemical and physical processes.[11–13] This is in stark contrast with chalcogenide quantum dots, which require complex, time-consuming, high-temperature syntheses to prepare the defect-free core–shell structures necessary for high PLQY.[14]

[a]School of Engineering, Faculty of Engineering and Physical Sciences, University of Southampton, Southampton SO17 1BJ, UK. E-mail: a.a.m.brown@soton.ac.uk
[b]Agency for Science and Technology Research (A*STAR) Singapore Institute of Manufacturing Technology (SIMTech), 73 Nanyang Drive, Singapore 637662, Republic of Singapore
[c]University of Southampton Malaysia, Iskandar Puteri 79200, Johor, Malaysia
[d]Energy Research Institute at NTU (ERI@N), Research Techno Plaza, X-Frontier Block Level 5, 50 Nanyang Drive, Singapore 637553, Republic of Singapore
[e]School of Materials Science and Engineering, Nanyang Technological University, 50 Nanyang Avenue, Singapore 639798, Republic of Singapore.
E-mail: Nripan@ntu.edu.sg

†Electronic supplementary information (ESI) available: Characterization methodology and additional characterisation studies. See DOI: 10.1039/c9nr02566a

All-inorganic cesium lead halide nanocrystals ($CsPbX_3$ NCs, X = I, Br, Cl) have attracted special attention, as they are more thermally stable and less moisture-sensitive than their hybrid counterparts, which contain organic methylammonium or formamidinium cations.[15,16] Hot-injection syntheses of $CsPbX_3$ NCs have generally employed ligands with long alkyl chains, oleic acid (OA) and oleylamine (OLAm), to passivate the nanocrystal surface,[17] in order to facilitate their colloidal dispersion in non-polar solvents. However, these ligands coordinate only weakly to the nanocrystal surface and are in a dynamic equilibrium between bound and unbound states.[18] As a result, the subsequent anti-solvent purification cycles, which are necessary to remove excess organic material from the NC ink, induce the desorption of oleylammonium bromide or oleate ion pairs, which creates anionic vacancies on the NC surface, drastically reducing the PLQY.[19,20] Furthermore, increasing surface passivation with long, insulating alkyl ligands inhibits the conductivity of thin-films deposited from the NC ink; this represents a trade-off that currently limits the achievable efficiency of $CsPbBr_3$ NC LEDs. It is therefore crucial to develop short, strongly-bound ligands that can also overcome the restrictions of dynamic binding equilibria.

$CsPbBr_3$ NCs were recently synthesized utilizing short octylphosphonic acid (OPA) ligands in combination with trioctylphosphine oxide (TOPO).[19] Remarkably improved antisolvent resistance was observed, thus, in contrast to the OA/OLAm ligand system, high PLQY could be retained through multiple purification cycles. This minimized the quantity of excess ligand in the final NC ink. LEDs fabricated based on this approach achieved a maximum external quantum efficiency (EQE) of 6.5%. Interestingly, the synthesis could not yield dispersible NCs if only TOPO was used. This implied that OPA was the effective ligand, a hypothesis backed up by recent work that indicates the inability of TOPO to bind to $CsPbBr_3$ NC surfaces.[21] The efficacy of phosphonic acid ligands was further elucidated by Nenon *et al.*, who demonstrated that hexylphosphonate ligands bound strongly to under-coordinated lead atoms exposed by surface bromide vacancies. Through density functional theory calculations, halide vacancies were revealed to be the predominant source of deleterious band-gap trap states, thus the capability of the phosphonate group to passivate these sites significantly enhanced the PLQY.[20]

Ligands with the phosphonic acid functionality, hence provide an upgrade on the ubiquitous oleic acid/oleylamine ligand system. However, the mechanism responsible for the stronger, more robust binding of phosphonic acids to $CsPbBr_3$ nanocrystals remains unexplained. Study of this mechanism is vital for understanding the outstanding solvent resistance and passivation afforded by phosphonates, and their contrasting behaviour relative to oleate ligands.

Herein, we describe a facile and effective post-synthetic ligand exchange protocol, whereby octylphosphonic acid was added to as-synthesized OA/OLAm-capped $CsPbBr_3$ NCs, initiating the binding of octylphosphonate ligands to the NC surface. Solid-state nuclear magnetic resonance (NMR) and Fourier Transform Infrared (FTIR) spectroscopy studies provided a mechanistic insight into the surface passivation, uncovering direct evidence that OPA ligands attach strongly to the surface of $CsPbBr_3$ nanocrystals. An effective antisolvent purification scheme initiated the self-assembly of a distribution of discrete monodentate OPA binding modes into a robust, extensive, hydrogen bonded network. The results suggest that octylphosphonates bound preferentially through $P–O^-$, such that consecutive adjacent octylphosphonate ligands can be connected through hydrogen bonding to form long inter-ligand chains. Highly efficient light-emitting diodes were fabricated incorporating post-treated NCs, achieving EQE of up to 7.74%. This efficiency presents a more than 2-fold improvement on the untreated NC devices, and is one of the highest reported values for all-inorganic $CsPbBr_3$ NC-based LEDs.

Results and discussion

Cesium lead bromide nanocrystals were synthesized according to the hot-injection method outlined by Protesescu *et al.*[17] Hot-injection was conducted at 170 °C and the reaction was quenched after 5 s. $CsPbBr_3$ NCs were also synthesized according to the method of Tan *et al.* (*in situ* OPA/TOPO synthesis),[19] to facilitate a comparison with the *ex situ* approach employed here. The resulting OPA/TOPO-capped $CsPbBr_3$ NCs were precipitated from the crude solution by centrifugation (OPA/TOPO-0w).

Scheme S1† depicts the purification and ligand exchange protocol developed for OA/OLAm-$CsPbBr_3$ NCs. Aprotic antisolvents were selected, as protic solvents can promote the formation of metal ions, thus degrading the NCs.[22] Based upon a previous report of its capability for effective purification of oleyl-capped $CsPbBr_3$ NCs, the medium polarity solvent ethyl acetate was selected as the first antisolvent.[22] Ethyl acetate (EtOAc) was added in a 3 : 1 volume ratio to the NC dispersion prior to centrifugation. This process was repeated with a 1 : 1 volume ratio of acetonitrile (ACN). Untreated and OPA-treated samples extracted after the first washing cycle were denoted as REF-1w and OPA-1w, whereas those extracted after the second washing cycle were referred to as REF-2w and OPA-2w, respectively.

Ligand exchange allowed efficient comparison of ligand binding and passivation efficacy. The size distribution, shape and surface termination structure of $CsPbBr_3$ NCs can all vary when the ligand system or synthetic method are altered. Thus analysing ligand binding to NCs synthesized identically in the same batch, according to a well-studied procedure, was a fairer, more accurate, and more reproducible approach.

The size distribution of the NCs in an OPA-2w dispersion in Fig. 1a was studied using a small-angle X-ray scattering (SAXS) method. The average NC edge length obtained was 10.1 ± 0.2 nm, which is consistent with transmission electron microscopy (TEM) images, shown in Fig. 1b and Fig. S1.† The absorbance and photoluminescence spectra for the fully purified OPA-modified NCs are shown in Fig. 1c. The concentration of the NC dispersion was 18 mM, calculated from the

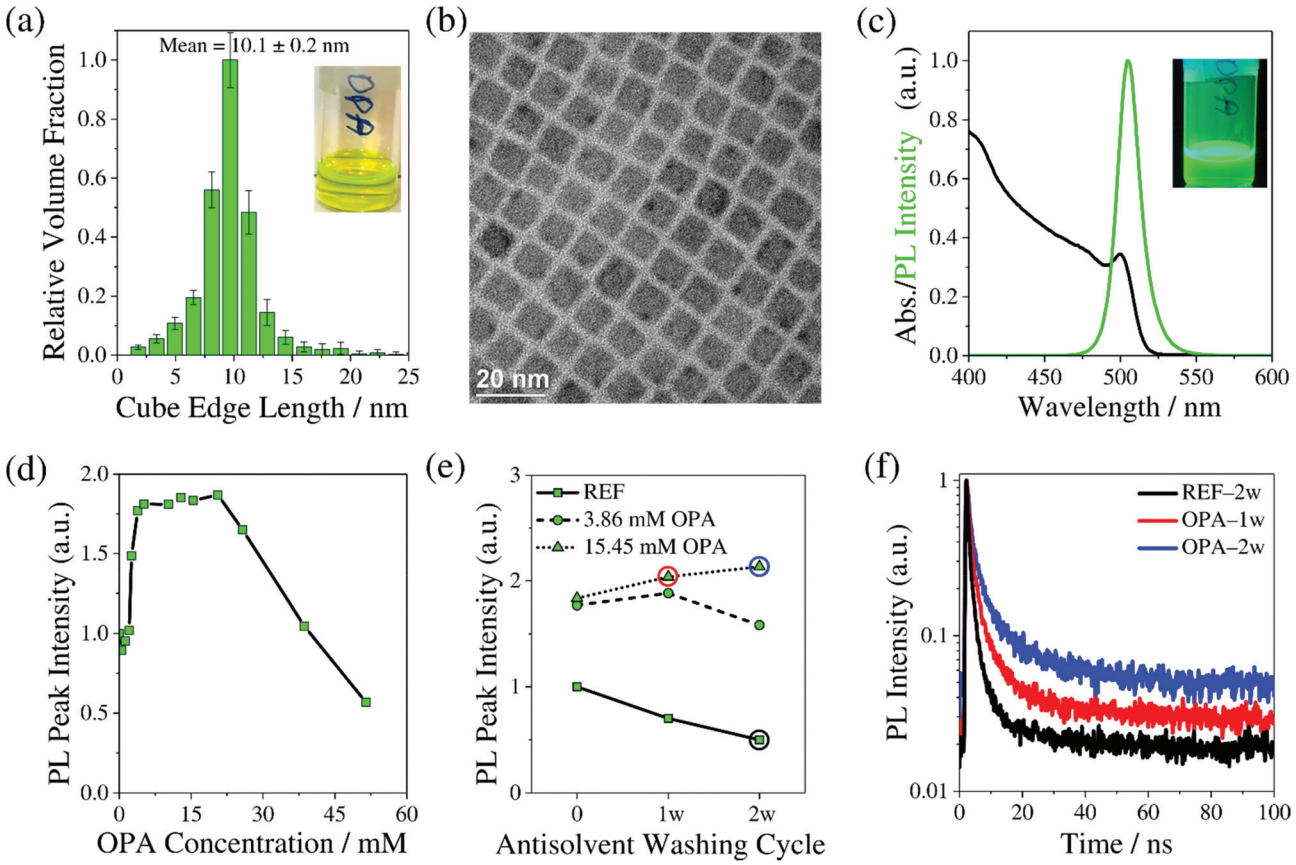

Fig. 1 $CsPbBr_3$ NC characterization. (a) NC edge length distribution derived from small-angle X-ray scattering (SAXS). Inset: Photograph of OPA-2w $CsPbBr_3$ NC dispersion (b) transmission electron microscopy image and (c) absorbance and PL spectra (λ_{ex} = 365 nm), of an OPA-2w NC dispersion. Inset: Photograph of OPA-2w $CsPbBr_3$ NC dispersion under UV illumination. (d) PL intensity maximum of a $CsPbBr_3$ NC dispersion as a function of the concentration of octylphosphonic acid solution added. (e) PL peak intensity of $CsPbBr_3$ NC toluene dispersions treated with low (3.86 mM/0.75 mg mL^{-1}) and high (15.45 mM/3 mg mL^{-1}) concentration OPA solutions before purification and after consecutive (1) 3 : 1 v/v ethyl acetate and (2) 1 : 1 v/v acetonitrile purification cycles. (f) Time-resolved PL decays at λ_{ex} = 405 nm of the 3 NC samples indicated by coloured circles in (e).

absorbance spectrum using an available $CsPbBr_3$ NC absorption coefficient.[23] Fig. 1d shows quantification of the photoluminescence intensity enhancement observed upon OPA treatment. The maximum photoluminescence, achieved with *ca.* 20 mM OPA, was almost 2 times higher than an untreated NC dispersion. The maximum PL intensity corresponds to a OPA : $CsPbBr_3$ molar ratio of approximately 1 : 1 (*ca.* 5000 ligands per NC). Fig. 1d shows three distinct passivation regimes; an initial steep increase of PL intensity with OPA concentrations up to *ca.* 4 mM, followed by a much more gradual increase between 4 and *ca.* 20 mM, and a rapid decrease as the concentration is increased further. This suggests that excess octylphosphonic acid ligands may have bound to different sites or by a different mechanism in the two regimes, such that the passivation efficacy in the second regime is much reduced. The degradation of photoluminescence above 20 mM could be attributed to the strength of the lead–phosphonate bond overcoming the crystal cohesive energy at higher phosphonate concentrations.[20] Alternatively, replacing too many oleyl ligands with octyl may destabilise the dispersion of 10 nm particles, leading to agglomeration, or there may be some phase transformation induced by excess acid; conversion of some $CsPbBr_3$ to weakly-fluorescent Cs_4PbBr_6 would reduce the photoluminescence intensity.[20] A significant proportion of weakly-bound ligands would be expected to detach from the nanocrystal surface during antisolvent purification. For [illegible]d systems targeted towards thin-film device application, it is important that effective defect passivation is retained in the ink used to deposit thin-films. Fig. 1e shows the photoluminescence spectra after each purification cycle for an untreated $CsPbBr_3$ NC dispersion and those treated with low (3.86 mM) and high (15.45 mM) OPA solution concentrations. These two concentrations provided comparable PL enhancement before purification and both showed an increase in PL intensity after EtOAc purification. However, there was a clear contrast after ACN purification; the PL of the NC dispersion treated with a high OPA concentration increased further, while it decreased for the low OPA concentration sample. This result indicates that a higher OPA concentration was important to the retention of photoluminescence through purification. The purified OPA-treated NC ink (15.45 mM OPA) displayed PL intensity *ca.* 4 times higher than the untreated control. This is

consistent with PLQY values measured for fully purified samples with OPA and without OPA, which were 62% and 20% respectively.

Fig. 1f shows time-resolved photoluminescence (TRPL) spectra of untreated reference (REF) and OPA-treated (OPA) NC films deposited from NC inks extracted after EtOAc (1w) and ACN (2w) washing steps (as depicted in Scheme S1†). The exciton lifetimes are well-described by a bi-exponential decay function. The non-radiative (τ_1) and radiative (τ_2) characteristic decay lifetimes were extracted from a bi-exponential fitting of the TRPL curves, and the average fluorescence lifetime (τ_{ave}) was calculated, taking into account their respective amplitudes (A_1 and A_2) (see Table S1†). The relative contributions of τ_1 and τ_2 were similar for all 3 samples.

REF-2w, OPA-1w and OPA-2w show τ_1 values of 0.78, 1.07 and 1.44 ns, respectively, while their relative amplitude remained similar. An increase of τ_1 upon OPA addition is consistent with the PL intensity enhancement observed (Fig. 1d), as it indicates a reduction of non-radiative recombination at the NC surface, which is attributable to improved surface defect passivation by OPA. OPA-2w has a higher τ_1 than OPA-1w, correlating well with Fig. 1e, which shows increased PL intensity after the 2nd wash (2w). The τ_2 values for REF-2w, OPA-1w and OPA-2w were 3.8, 6.1 and 10.3 ns, respectively. An increase of the radiative lifetime of the exciton indicates a reduction of the ligand density in the film. Thus, an increase of τ_2 with OPA addition implies that shorter OPA ligands replaced long oleyl ligands, reducing the total insulating organic content in the film. The increase of τ_2 from OPA-1w to OPA-2w demonstrates that the second purification step with ACN removed a significant quantity of excess ligand from the NC ink. Overall, TRPL provided evidence that OPA-treatment replaced oleyl ligands, more effectively passivating the surface of $CsPbBr_3$ NCs, and this passivation was maintained while ACN removes a substantial quantity of excess ligand material.

Thermogravimetric analysis (TGA) was conducted on powders of all 4 NC samples. Plots of weight loss with temperature up to 550 °C are presented in Fig. S2.† The weight loss between 200 and 300 °C is less severe for the OPA samples, which can be attributed to lesser quantities of oleyl ligands. The OPA samples both show a steep weight loss between 400 and 500 °C, which we assign as the decomposition of OPA ligands, as a similar feature was observed by Tan *et al.* for OPA/TOPO-$CsPbBr_3$ NCs.[19] The continued weight loss beyond 500 °C corresponds to the decomposition of the $CsPbBr_3$ NCs. These results demonstrate that OPA ligands improve the thermal stability of $CsPbBr_3$ NCs. In addition to thermal stability, the photoluminescence spectra of dilute OPA-2w and REF-2w solutions were measured over 8 days (Fig. S3†). The PL of the OPA-treated sample showed no broadening or change in peak position, whereas the PL emission of the untreated sample exhibited red-shift of *ca.* 7 nm and a clear increase of the FWHM. OPA clearly improves colloidal stability, which suggests that it binds more strongly and thus, is less susceptible to desorption, than OA and OLAm ligands.

Solid-state magic-angle spinning NMR (ssNMR) was conducted on REF-1w, REF-2w, OPA-1w, and OPA-2w precipitates, collected as depicted in Scheme S1.† An OPA/TOPO-0w sample was also analysed by ssNMR, as were crystalline OPA and TOPO samples for reference. Solid-state NMR provides insight which is complementary to the solution NMR techniques often employed in the study of nanocrystals. In the solid state, an accurate representation of ligand binding in the nanocrystal films of optoelectronic devices can be obtained, whereas solution NMR analyses NCs in colloidal suspension prior to [illegible]pating. The ^{13}C NMR spectra for all samples is displayed in [illegible]g. S4.† There was no evidence of carboxylic acid functional groups (–COOH, approx. 180 ppm) in the ^{13}C spectra of the OPA modified samples. This is in agreement with previous studies which asserted that oleate ligands do not bind to the surface of $CsPbBr_3$,[18,24] and demonstrates that octylphosphonate ligands passivated surface sites which oleate ligands were unable to. There remained a prominent oleylamine signal in the OPA-treated samples however, indicating there was no substantial loss of oleylamine from the nanocrystal surface.

The ^{31}P proton-decoupled NMR spectra for each of the OPA-modified precipitates are shown above their respective ^{31}P–^{1}H heteronuclear correlation (HETCOR) 2D NMR data in Fig. 2. The ^{31}P spectrum of OPA-1w displays 4 resonances that are paired in 2 distinct environments, centred around 32 and 25 ppm, respectively. These environments were shifted upfield from the crystalline OPA resonance at 37.5 ppm. [illegible]iple literature studies have observed similar analogous upfield ^{31}P shifts in phosphonic acid ligands bonded to metallic oxide surfaces.[25,26] Thus, the shift of the ^{31}P resonance indicates that OPA has bound to the surface of $CsPbBr_3$ NCs. Typically, neutral phosphonic acid ligands are found to have smaller shifts, while deprotonated phosphonate ligands produce larger shifts, corresponding to the degree of deprotonation. Larger shifts upon ligand binding have been considered an indication of stronger ligand–metal interaction.[27] Although previous literature reports considered systems involving various alkylphosphonic acid ligands and a range of different surfaces, the chemical shifts described can nonetheless inform the assignments of the ^{31}P data in this study. Based upon literature assignments attributing significant shifts to deprotonation of the phosphonic acid, the environment about 32.0 ppm ($\Delta\delta$ approx. −5 ppm) is assigned as OPA binding through neutral octylphosphonic acid molecules (OPA), whereas the environment around 25 ppm ($\Delta\delta$ approx. −12 ppm) was attributed to monoionic octylphosphonate binding (OPA^-).[25,27] Previous studies of phosphonic acid ligands, on chalcogenide and metal oxide nanoparticles, have indicated that binding to divalent metal sites occurs preferentially through the X-type hydrogen phosphonate anion, rather than a neutral dative (L-type) bond.[28–30] Furthermore, De Keukeleere *et al.* suggest that phosphonate species coordinated to Lewis acidic metal sites are better stabilised than the phosphonic acids.[30]

The small splitting of each resonance into pairs was attributed to two different binding modes possible for both octylpho-

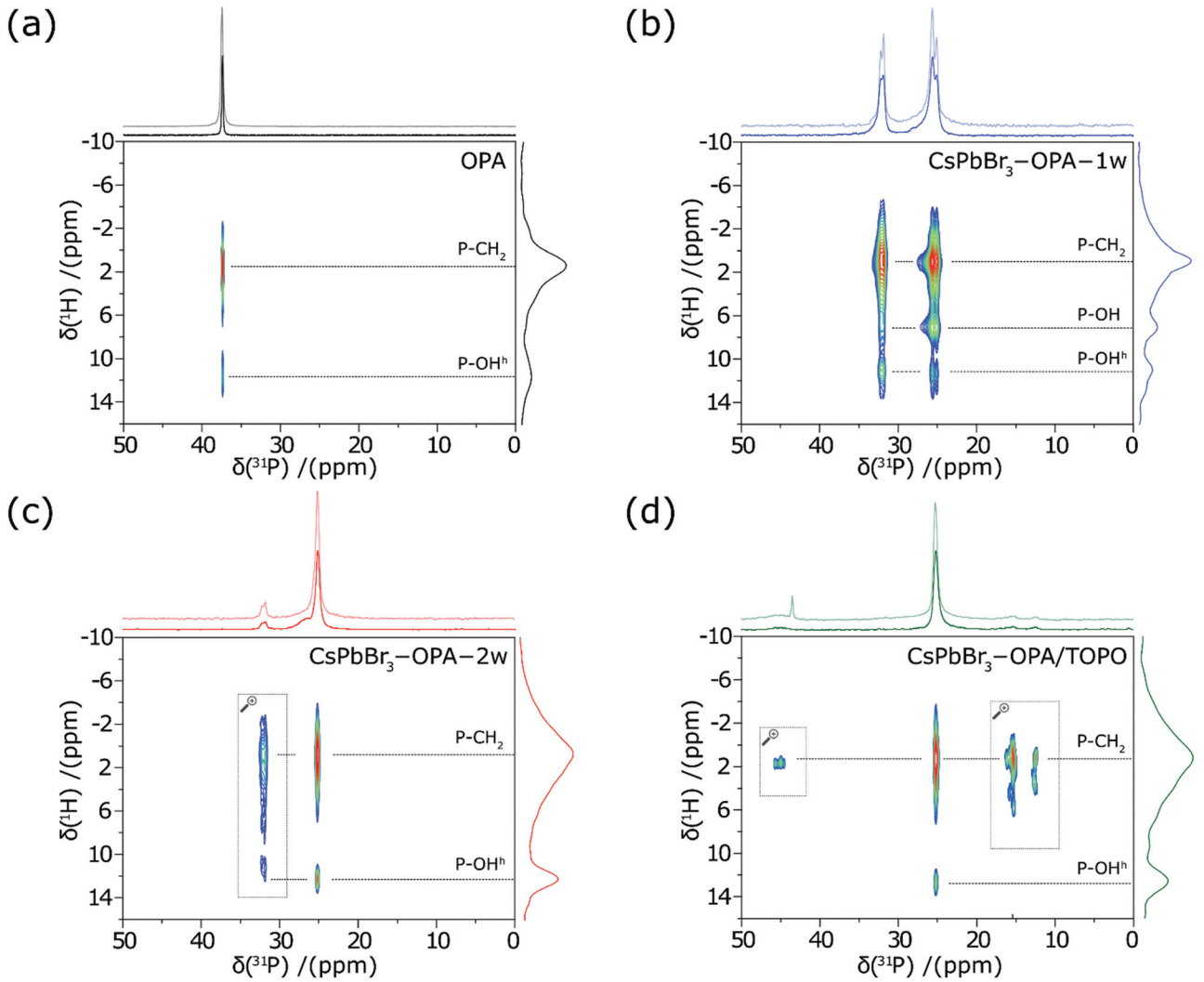

Fig. 2 ^{31}P–^{1}H HETCOR ssNMR spectra of (a) crystalline OPA reference, (b) $CsPbBr_3$ NCs treated with OPA after ethyl acetate and (c) acetonitrile purification cycles, and (d) unpurified $CsPbBr_3$ NCs synthesized using OPA and TOPO. The 1D ^{31}P MAS NMR spectrum is shown above each 2D HETCOR spectrum for comparison. Areas marked by 🔍 have magnified contour levels to reveal the detail of lower intensity HETCOR resonances.

sphonic acid and octylphosphonate. It is hypothesized that the two resonances about 32.0 ppm correspond to the coordination of neutral OPA to the nanocrystal surface as a Lewis base through the lone pair on the oxygen atom of either P=O or P–OH. Similar shifts have previously been assigned to the physisorption of methylphosphonic acid through P=O to silica nanoparticles.[25] Deprotonation of these coordinated neutral ligands then leads to two possible monoionic octylphosphonate binding modes. The proposed mechanism is outlined in Scheme 1. Deprotonation of OPA coordinated to the NC surface through P–O(H) is expected to occur preferentially at the bound P–OH, as coordination of the oxygen atom to the NC surface weakens the O–H bond. Thus two, rather than three, major resonances were observed around 25 ppm. All ^{31}P NMR assignments are listed in Table 1.

Multiple ^{31}P resonances for a single phosphonic acid ligand were previously reported for CdSe nanomaterials. These were attributed to different binding strengths for adsorption of phosphonate ligands to different facets of the wurtzite crystal structure.[28] The cubic structure of $CsPbBr_3$ NCs presents with 6 CsBr-terminated facets, thus analogous reasoning cannot apply here.[31] Moreover, *in situ* synthesis of OPA-capped $CsPbBr_3$ NCs yields spherical nanocrystals, rather than anisotropic structures that would be expected if OPA displayed some facet selectivity.[32]

Nenon *et al.* have shown that, owing to the relative chemical softness of phosphonic acids, and in contrast to oleate species, phosphonic acids can interact sufficiently with undercoordinated Pb atoms to fill halide vacancies at the NC surface.[20] This correlates well with the observation made by Smock *et al.* that phosphonic acid ligands do not participate in a binding equilibrium when introduced to a OA/OLA-$CsPbBr_3$ NC dispersion, instead they bind irreversibly to the surface.[33] As OLA deprotonates OPA species, the OA/OLA and HBr/OLA equilibria can be expected to shift towards the left (unbound species) based on Le Chatelier's principle, as

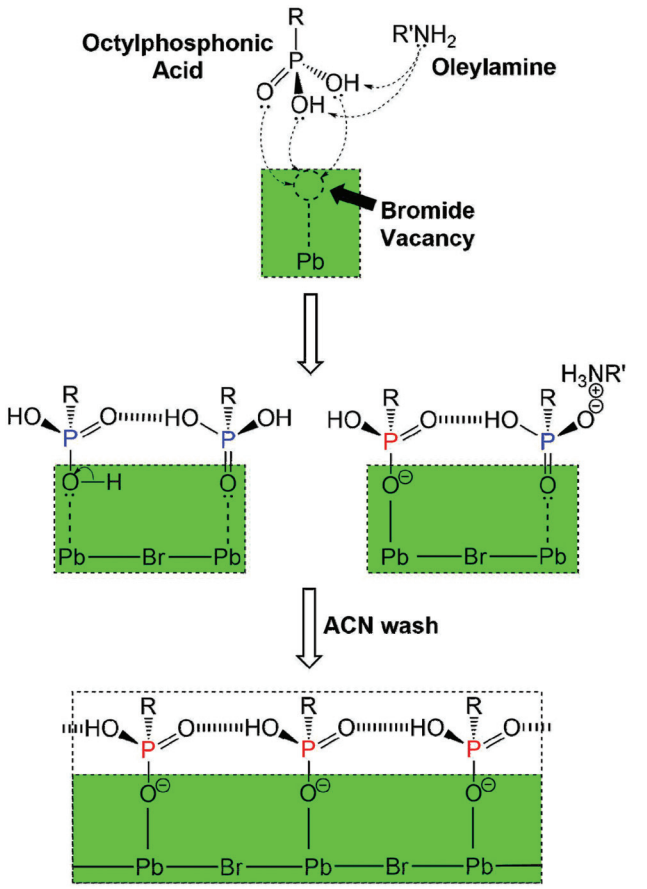

Scheme 1 Proposed attachment mechanism of octylphosphonic acid ligands to the surface of $CsPbBr_3$ NCs (R = octyl, R′ = oleyl). The Pb–Br–Pb linkages represent corner sharing $[PbBr_6]^{4-}$ octahedra of the perovskite lattice.

Table 1 ^{31}P chemical shift assignments for different ligands and degrees of binding to $CsPbBr_3$ NCs

Ligand	δ_{iso} (^{31}P) (ppm)	$\Delta\delta$ (ppm)
OPA, free	37.5 ± 0.1	0
OPA, bound	32.2 ± 0.1	−5.3
	31.8 ± 0.1	−5.7
OPA^-, bound	25.6 ± 0.1	−11.9
	25.1 ± 0.1	−12.4
OPA^{2-}, bound	15.4 ± 0.3	−22.1
	12.5 ± 0.2	−25.0
TOPO, free	47.9 ± 0.1	0
TOPO, bound	43.5 ± 0.1	−4.4

the resulting octylphosphonate species are effectively removed from the system on account of their irreversible binding to the NC surface. As more bound oleylammonium is converted to free oleylamine, further OPA molecules can be deprotonated; thus establishing a synergetic process (Scheme 2). This process would maintain the oleylammonium concentration but reduce the oleate and bromide concentrations.

Once octylphosphonate ligands have bound to all accessible sites on the NC surface, further octylphosphonate species generated would be expected to remain free in solution. This supposition correlates well with the second regime observed in Fig. 1b, where a plateau in the PL intensity was observed. Free, unbound OPA likely participates in an acid–base equilibrium with oleylamine. Thus when polar solvent purification causes desorption of oleylammonium bromide or oleate species, the remaining excess octylphosphonate species could fill the newly created halide vacancies. This provides a rationalization for the improvement of photoluminescence intensity after ACN washing when the higher OPA concentration was employed (Fig. 1e).

[1] $RPO(OH)_2 + R'NH_2 \rightarrow RPO(OH)O^- + R'NH_3^+$

[2] $R'COOH + R'NH_2 \leftrightharpoons R'COO^- + R'NH_3^+$

[3] $HBr + R'NH_2 \leftrightharpoons Br^- + R'NH_3^+$

Scheme 2 [1] The deprotonation of octylphosphonic acid by oleylamine, [2] & [3] acid–base equilibria of species on the surface of $CsPbBr_3$ nanocrystals (R = octyl, R′ = oleyl).

The ^{31}P–^1H HETCOR data in Fig. 2 shows the through space correlation of ^{31}P sites to all nearby ^1H environments. All ^{31}P resonances were close to 3 distinct ^1H environments centred at δ = 1, 7 and 11 ppm, respectively. The largest resonance at δ = 1 ppm was due to the P–CH_2 correlation from the octyl chain, while the other two resonances represent the P–OH group. The signal at δ = 7 ppm was attributed to free P–OH and the signal at δ = 11 ppm was due to hydrogen bonding (P–OH^h) to a nearby electronegative site.[25] The ^1H chemical shift positions of P–OH^h are well known; ^1H chemical shifts of δ = 9.9 to 16.0 ppm have previously been observed for hydrogen bonds, where the higher chemical shifts corresponded to shorter bond lengths.[34] The presence of P–OH groups in the ligand environment ruled out complete deprotonation of OPA. ^{31}P resonances for multidentate binding modes are typically found below 20 ppm;[25] as evidenced by the HETCOR spectra for the NCs synthesized with OPA/TOPO (*i.e.* small features visible at δ = 16 ppm and δ = 13 ppm in Fig. 2d). No hydrogen bonded P–OH correlations were observed for these resonances, which is consistent with complete deprotonation.

Due to the presence of P–OH^h resonances, it is believed that for all observed binding configurations hydrogen bonding occurred between P–OH and P=O sites on adjacent OPA ligands. This hypothesis is strongly supported by the very narrow resonances, which are indicative of long-range order. Typically, the ^{31}P signals for phosphonic acid ligand binding are much broader, indicating a wide distribution of binding geometries and orientations.[35,36] In order for adjacent OPA ligands to form hydrogen bonds between one another, they must align themselves into a consistent orientation, with every ligand in the chain exhibiting similar phosphorus environments, and thus similar ^{31}P chemical shifts. It is notable that $CsPbBr_3$ has a very ionic lattice, such that binding strength to its surface is not expected to be strongly dependent on orbital overlap, and by extension, ligand orientation. Thus, maximization of ligand–metal orbital overlap is unlikely to drive the

extensive ligand alignment indicated by the ssNMR results, particularly when such alignment was not observed for less ionic materials. To the best of our knowledge, hydrogen bonding between bound phosphonic acid ligands has not previously been observed. This may be attributable to the particularly large distance (~6 Å) between binding sites on the perovskite surface.[37] On metal oxide and chalcogenide NCs, adjacent binding sites are closer together, and consequently, bridging of multiple sites by a single phosphonic acid molecule are typically observed instead.[38]

For sample OPA-1w, comparison of the relative intensities of the ^{1}H resonances at 7 and 11 ppm (Fig. 2b) reveals that a proportion of P–OH hydrogens did not participate in hydrogen bonding. Therefore, we believe the OPA ligands formed pairs or piecemeal groups across the NC surface, leaving a significant fraction of bound species with a free (*i.e.* not hydrogen bonding) P–OH group. For sample OPA-2w, the intensity of the neutral OPA environment centred at δ = 32.0 ppm had significantly reduced, whereas the lower frequency monoionic environment had grown concurrently; presenting only one significant resonance at 25.2 ppm. This suggests that an additional purification cycle preferentially removed OPA corresponding to three out of the four possible binding resonances. This may be attributable to the ionic interaction of P–O^{-} with the highly ionic perovskite lattice. This mode should be the most strongly-bound, and thus more resistant to breakage during the acetonitrile washing step than the other, Lewis base-type, binding modes. The ^{31}P–^{1}H HETCOR data shows that the P–OH groups correlated to this single remaining intense OPA resonance were predominantly hydrogen bonded, unlike in OPA-1w, as the P–OH resonance at δ = 7 ppm is no longer present, whereas the P–OH^{h} resonance remains at δ = 12.2 ppm. As any terminal OPA molecules of an inter-ligand hydrogen bonded network would have a free P–OH, this suggests that the network has become more extensive (*i.e.* fewer terminal P–OH). A potential explanation for this would be the reconfiguration of weaker binding modes into the tighter-bound hydrogen binding network. There is little change in the organic ligand content of OPA-1w and 2w, according to the TGA results (Fig. S2†), which provides evidence for OPA reconfiguration rather than the complete removal of OPA bound by the 3 weaker modes. The increased non-radiative exciton lifetime (τ_1) upon ACN purification (Fig. 1f) further corroborates this ligand reassembly, as it indicates that the second washing step with acetonitrile actually improved defect passivation.

The resonance at δ = 7 ppm could alternatively be assigned to an interaction between oleylammonium and P, with the depletion of this signal upon ACN washing attributable to oleylammonium desorption. However, the ^{13}C NMR spectra of OPA-1w and OPA-2w (Fig. S4†) rule out this hypothesis, as oleylamine is observed in both samples (the resonance around 42 ppm corresponds to the R–C[H$_2$]–NH$_2$ protons of OLA) and hence no significant loss of bound OLA occurred.

The purification step with more polar ACN (as opposed to ethyl acetate) may break the weaker interactions between OPA and the NC surface. Moreover, the ACN can act as a Lewis base, thus it may also compete with the Lewis base-type OPA binding modes. Two adjacent OPA ligands coordinated through P=O cannot form a hydrogen bond as there are no free P=O groups. Therefore this reconfiguration would mean that the vast majority of bound OPA ligands are now capable of forming two hydrogen bonds. This facilitates the extension of the existing scaffold of short OPA chains, establishing a far more extensive hydrogen bonded network, as indicated by the OPA-2w HETCOR spectrum in Fig. 2c. Further, the desorption of some weakly-bound oleylammonium bromide ligand pairs due to ACN purification may also have aided the continuity of OPA chains as further halide vacancies, and therefore further sites for octylphosphonate binding, would be created.

The ^{31}P–^{1}H HETCOR data for the OPA/TOPO sample exhibited a single significant resonance at δ ~25 ppm, with predominantly hydrogen bonded P–OH groups. This matches well with the position and intensity of the main resonance peak observed for sample OPA-2w. Therefore the ligand exchange and purification protocol reported here yielded comparably bound octylphosphonate ligands to the *in situ* synthetic approach. The OPA/TOPO sample exhibited a single binding mode without purification, implying that this mode is the most energetically favourable. We note that it is highly likely that a hydrogen-bonded network of octylphosphonate ligands is responsible for the exceptional stability and ethanol tolerance reported for OPA/TOPO CsPbBr$_3$ NCs.[19] This conclusion demonstrates that monitoring ligand attachment at room temperature can unveil details of the binding mechanism which are concealed by the fast kinetics of the hot-injection synthesis.

The similarity of the P–OH^{h} proton resonance from the OPA/TOPO synthesis, where oleylamine is not used, and our OPA-modified samples ruled out any inter-ligand hydrogen bonding between octylphosphonate and oleylammonium. It is theoretically feasible that the ligands' P–OH groups could be interacting with nearby Br^{-} ions rather than the P=O groups of adjacent ligands.[39] However, the assumption that OPA ligands form hydrogen bonds among one another rather than with Br^{-}, is corroborated by comparing the P–OH^{h} correlation in the pure OPA crystal. Here, the OPA crystal structure is formed *via* OPA molecules hydrogen bonding to each other, giving rise to a P–OH^{h} proton resonance at a very similar chemical shift (Fig. 2a, δ_{iso} = 11.6 ppm) as found for the OPA ligands on CsPbBr$_3$ NCs. In the absence of any evidence supporting hydrogen bonding to Br^{-}, we confidently assert that adjacent OPA ligands were hydrogen bonded.

To complement the ssNMR analysis, attenuated total reflection (ATR) FTIR was conducted on the same samples (Fig. S5†). The appearance of strong bands in the P–O region, the concurrent reduction of the carbonyl stretch around 1700 cm^{-1} and, most obviously, the two metal carboxylate bands around 1524 and 1402 cm^{-1}, provide further evidence for the removal of oleate species and binding of octylphosphonates.[40] This is consistent with the absence of –COOH signals

in the ^{13}C NMR spectra, and increased exciton lifetimes obtained from TRPL spectra, for OPA-modified samples.

LED devices were fabricated in order to demonstrate the promising applications of $CsPbBr_3$ NCs capped by an octylphosphonate ligand network. The structure employed was: indium tin oxide (ITO)/poly(3,4-ethylenedioxythiophene):poly(styrenesulfonate) (PEDOT:PSS, 40 nm)/$CsPbBr_3$ NCs (40 nm)/2,4,6-tris[3-(diphenylphosphinyl)phenyl]-1,3,5-triazine (POT2T, 45 nm)/calcium (Ca, 7 nm)/aluminium (Al, 100 nm). The band diagram in Fig. 3a outlines the energy level alignment of the various stack components. A detailed description of the device fabrication can be found in the Methods section.

Fig. 3b–d shows the device characteristics of LEDs fabricated with 4 different $CsPbBr_3$ NC inks; REF-1w, OPA-1w, REF-2w and OPA-2w. Fig. 3b shows that the OPA-2w device have a lower turn on voltage of 2.6 V (at 1 cd m^{-2}), compared to 2.8 V and 3 V for REF-2w and both 1w samples, respectively. Plots of EQE against current density are displayed in Fig. 3c; OPA-2w device achieved a maximum EQE of 7.74%, remarkably higher than the REF-2w, OPA-1w and REF-1w devices, which showed maximum EQEs of 3.59%, 1.98% and 1.84% respectively. This represents a doubling of the efficiency with an octylphosphonate ligand network, and emphasizes the importance of the second, ACN purification step. The contrast between the EQE of OPA-1w and OPA-2w can be attributed to the rearrangement of OPA ligands into a single dominant strongly-bound mode upon ACN purification, as evidenced by HETCOR ^{31}P–^{1}H NMR in Fig. 2b and c. The removal of weakly-bound OPA ligands reduced the proportion of insulating organic material in the film, which contribute to film resistivity without significantly passivating under-coordinated lead sites. Removal of excess OLAm and OA likely contributed to the improved LED efficiency too, as REF-2w achieved significantly higher EQE than both 1w samples. The reduced non-radiative recombination afforded by the purification regime employed is corroborated by high efficiency at low luminance. Fig. 3d demonstrates that the power efficiency of the OPA-2w device peaked at 5 cd m^{-2} (21.74 lm W^{-1}), achieving EQE of 7.01% at 100 cd m^{-2}. The maximum luminance values observed were 1022 cd m^{-2} for OPA-2w, 229 cd m^{-2} for REF-2w, 185 cd m^{-2} for OPA-1w and 105 cd m^{-2} for REF-1w.

The performance of our LED devices here exceeds that reported for the *in situ* OPA-$CsPbBr_3$ NCs of Tan *et al.*[19] The ^{31}P–^{1}H HETCOR NMR spectra in Fig. 2c and d demonstrate that the surface passivation afforded by both methods was comparable, therefore we attribute the performance difference to the high dispersability afforded by retained oleylamine ligands. This enabled a more concentrated NC ink, which may

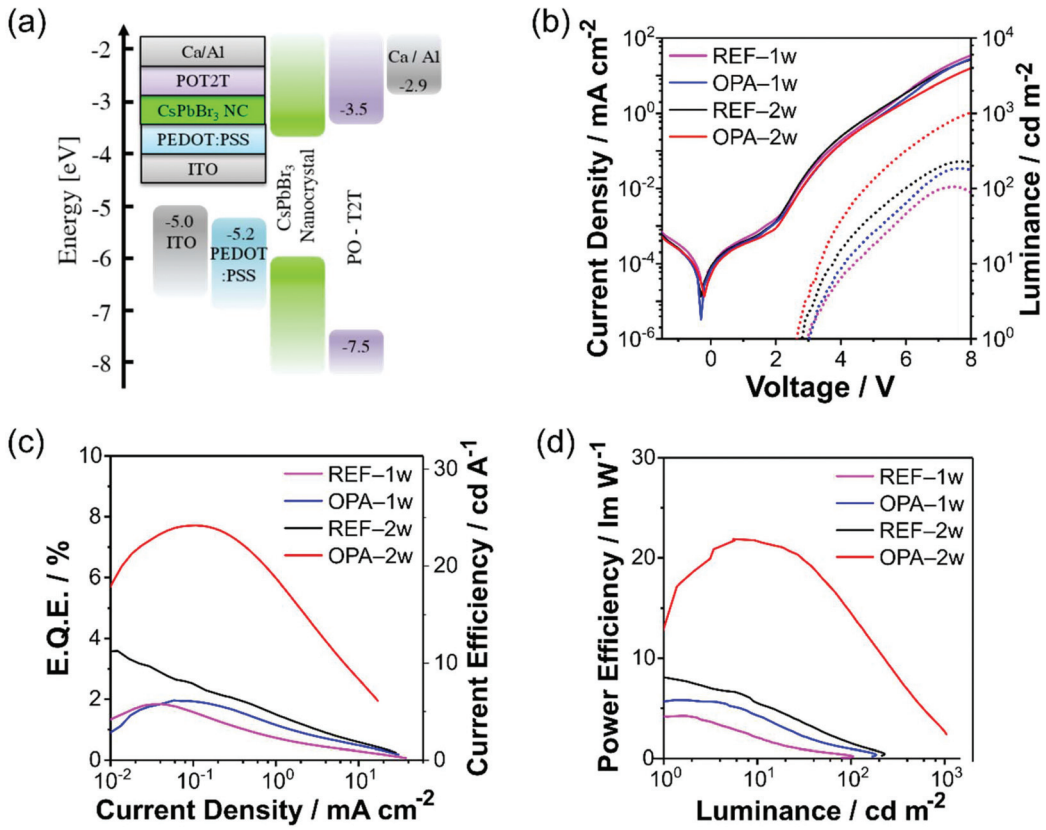

Fig. 3 $CsPbBr_3$ NC LED device characteristics. (a) Band diagram, (b) current–voltage–luminance, (c) EQE/current efficiency against current density, and (d) power efficiency against luminance plots. CON denotes reference NC inks, OPA denotes OPA-treated inks; 1w and 2w denotes inks washed once (EtOAc) and twice (EtOAc, ACN), respectively.

promote the deposition of more compact NC thin films. Another implication of this is that the efficiency of phosphonate-capped $CsPbBr_3$ NCs may be improved further if dispersability issues can be overcome without employing ligands with long insulating alkyl chains.

Conclusion

The ultimate objective of this study was to elucidate the properties of tightly–bound alkylphosphonate ligands on $CsPbBr_3$ NCs, thereby revealing a route to higher efficiency LEDs. Previous reports have speculated that the strong binding of alkylphosphonic acids could be attributed their capacity for multidentate coordination. On the contrary, we revealed herein that octylphosphonic acid binds preferentially to $CsPbBr_3$ NCs through a monodentate octylphosphonate mode. In this mode, the otherwise uncoordinated P–OH and P═O groups drive the self-assembly of a hydrogen-bonded inter-ligand network. We fabricated high-efficiency LEDs to demonstrate that this ligand network provides strong passivation of the perovskite lattice.

This work employs a mixed-ligand system, where the colloidal and environmental stability afforded by the octylphosphonate binding network cannot be accurately assessed due to the presence of other, dynamically-bound species on the NC surface. Nonetheless, the tightly-bound self-assembled ligand network offers a promising approach to protect the perovskite surface while strongly passivating defects, with potential relevance across the breadth of halide perovskite optoelectronic applications. The inter-ligand hydrogen bonding unveiled represents a novel feature, which has not previously been reported for any other ligand on any perovskite surface or interface. In addition to the obvious application for other perovskite nanocrystal compositions, this phenomenon could potentially be exploited to passivate lead defects at the perovskite interface in various thin-film devices.

Experimental

Chemicals

Lead bromide ($PbBr_2$, ≥98%), cesium carbonate (Cs_2CO_3, 99.9% trace metals basis), 1-octadecene (ODE, 90%), oleic acid (OA, 90%), oleylamine (OLA, 70%), octylphosphonic acid (OPA, 98%), trioctylphosphine oxide (TOPO, 99%), toluene (anhydrous, 99.8%), ethyl acetate (anhydrous, 99.8%) and acetonitrile (anhydrous, 99.8%) were all purchased from Sigma-Aldrich. All chemicals were used without further purification.

OA and OLA were dried separately under vacuum at 120 °C for a minimum of 2 hours before use.

Cs(oleate) preparation

Cs_2CO_3 (0.41 mmol, 0.268 g) and ODE (10 mL) were dried under vacuum at 120 °C for 30 min. Dried OA (3.16 mmol, 1 mL) was added under nitrogen and the solution was dried under vacuum at 120 °C for 90 min. The solution was then heated at 140 °C under nitrogen for 30 min to ensure complete formation of Cs(oleate). The Cs(oleate) solution was kept at 120 °C under vacuum until required.

$CsPbBr_3$ NC synthesis

OA/OLA-$CsPbBr_3$ NCs were synthesized according to a previously reported method.[17] $PbBr_2$ (0.38 mmol, 0.138 g) and ODE (10 mL) were dried under vacuum at 120 °C for 15 min. Dried OA (3.16 mmol, 1 mL) and dried OLAm (3.02 mmol, 1 mL) were added under nitrogen and the solution was dried under vacuum at 120 °C for 60 min. The $PbBr_2$ solution was heated to 170 °C under nitrogen. 0.8 mL Cs(oleate) was swiftly injected into the $PbBr_2$ solution with vigorous stirring and the reaction was quenched after 5 s in an ice water bath, with vigorous swirling to promote homogenous cooling.

OPA/TOPO-$CsPbBr_3$ NCs were synthesized according to a previously reported method.[19] The method was the same as for OA/OLA-$CsPbBr_3$ NCs, except OPA (1.03 mmol, 0.2 g) and TOPO (5.17 mmol, 2 g) replaced OA and OLAm.

$CsPbBr_3$ NC purification

For OA/OLA-$CsPbBr_3$ NCs, 12.5 mL crude NC dispersion was centrifuged for 10 min at 7000*g*. The precipitate was redispersed in 2.5 mL toluene and centrifuged for 10 min at 2500*g*. The precipitate was discarded and the supernatant was retained for antisolvent washing. For ligand-exchanged samples, a solution of OPA in toluene (concentration varied) was added at v/v to the NC dispersion. For untreated reference sample. mL toluene was added instead of OPA solution. 15 mL ethyl acetate was added to the $CsPbBr_3$ dispersion and the mixture was centrifuged for 10 min at 7000*g*. The precipitate was redispersed in 2.5 mL toluene and centrifuged for 10 min at 2500*g*. The precipitate was discarded and the supernatant was retained. 2.5 mL acetonitrile was added to the toluene dispersion and the mixture was centrifuged for 10 min at 7000*g*. The precipitate was redispersed in 1.25 mL toluene and centrifuged for 10 min at 2500*g*. The resulting supernatant was used as the NC ink for LED fabrication.

LED device fabrication

Pre-etched indium–tin oxide (ITO) glass substrates (sheet resistance of 8 Ω cm^{-1}) were washed under sonication in: detergent solution (10% v/v in deionized water), deionized water, acetone and twice in isopropanol, consecutively. The substrates were dried and treated for 15 min by UV-ozone. PEDOT:PSS (Clevios Al4083) was filtered with a (0.45 μm PVDF filter) and spin coated for 1 min at 4000 rpm (acceleration = 200 rpm s^{-1}) and thermally annealed for 10 min at 130 °C to remove any residual solvent. The substrates were transferred into an argon-filled glovebox for the remainder of the fabrication processes. $CsPbBr_3$ NC inks were drop-cast onto PEDOT:PSS, and after a 3 minutes delay, were spin coated for 1 min at 2000 rpm (acceleration = 250 rpm s^{-1}). 2,4,6-Tris[3-(diphenylphosphinyl)phenyl]-1,3,5-triazine (POT2T) was thermally evaporated under high vacuum (10^{-6} Torr) to achieve a thickness of 45 nm. Ca (7 nm) and Al (100 nm) were sequentially thermally

evaporated through a metal shadow mask. The active area of all devices used herein was 3 mm^2.

Author contributions

A. A. M. B. and S. V. conceived the idea for the manuscript and designed the experiments. A. A. M. B. performed the NC preparation. T. J. N. H. conducted the solid-state NMR characterization. A. B. performed the TRPL characterization. P. V. conducted thermogravimetric analysis. A. A. M. B. and X. Y. C. prepared and characterized the LEDs. The manuscript was led by A. A. M. B. and T. J. N. H., and contributed to by all authors. N. M. and S. G. M. led the project.

Conflicts of interest

There are no conflicts to declare.

Acknowledgements

A. A. M. B. gratefully acknowledges the Tizard studentship from Faculty of Engineering and Physical Sciences at University of Southampton, and the ARAP Scholarship from A*STAR.

This research was also supported by the National Research Foundation, Prime Minister's Office, Singapore, under its Competitive Research Program (CRP Award No. NRF-CRP14-2014-03).

References

1 K. Lin, J. Xing, L. N. Quan, F. P. G. de Arquer, X. Gong, J. Lu, L. Xie, W. Zhao, D. Zhang, C. Yan, W. Li, X. Liu, Y. Lu, J. Kirman, E. H. Sargent, Q. Xiong and Z. Wei, *Nature*, 2018, **562**, 245–248.

2 Y. Cao, K. Pan, Y. Ke, H. Tian, Y. Wang, M. Xu, Y. Wei, D. Kong, W. Zou, Q. Peng, N. Wang, J. Guo, K. Du, M. Yang, Y. He, H. Li, D. Dai, G. Li, H. Chen, H. Cao, Y. Jin, Z. Fu, Y. Miao, J. Wang and W. Huang, *Nature*, 2018, **562**, 249–253.

3 T. Chiba, Y. Hayashi, H. Ebe, K. Hoshi, J. Sato, S. Sato, Y. J. Pu, S. Ohisa and J. Kido, *Nat. Photonics*, 2018, **12**, 681–687.

4 J. Xing, Y. Zhao, M. Askerka, L. N. Quan, X. Gong, W. Zhao, J. Zhao, H. Tan, G. Long, L. Gao, Z. Yang, O. Voznyy, J. Tang, Z. H. Lu, Q. Xiong and E. H. Sargent, *Nat. Commun.*, 2018, **9**, 1–8.

5 J. Pan, Y. Shang, J. Yin, M. De Bastiani, W. Peng, I. Dursun, L. Sinatra, A. M. El-Zohry, M. N. Hedhili, A. H. Emwas, O. F. Mohammed, Z. Ning and O. M. Bakr, *J. Am. Chem. Soc.*, 2018, **140**, 562–565.

6 G. Li, J. Huang, H. Zhu, Y. Li, J. X. Tang and Y. Jiang, *Chem. Mater.*, 2018, **30**, 6099–6107.

7 S. Lilliu, N. C. Greenham, S. Bai, X.-J. She, R. H. Friend, D. Di, J. Wang, M. Alsari, L. Yang, B. Zhao, V. Kim, J. Zhang, L. Liang, H. J. Snaith, P. Gao, R. Shivanna, R. Lamboll, F. Auras, J. M. Richter and L. Dai, *Nat. Photonics*, 2018, **12**, 783–789.

8 G. Xing, B. Wu, X. Wu, M. Li, B. Du, Q. Wei, J. Guo, E. K. L. Yeow, T. C. Sum and W. Huang, *Nat. Commun.*, 2017, **8**, 14558.

9 H. Huang, M. I. Bodnarchuk, S. V. Kershaw, M. V. Kovalenko and A. L. Rogach, *ACS Energy Lett.*, 2017, **2**, 2071–2083.

10 J. Kang and L. W. Wang, *J. Phys. Chem. Lett.*, 2017, **8**, 489–493.

11 O. Nazarenko, L. Protesescu, M. V. Kovalenko, D. N. Dirin and S. Yakunin, *ACS Appl. Nano Mater.*, 2018, **1**, 1300–1308.

12 B. Han, Q. Shan, H. Zeng, J. Li, L. Xu, J. Li, F. Zhang and J. Song, *Adv. Mater.*, 2018, **30**, 1800764.

13 X. Y. Chin, A. Perumal, A. Bruno, N. Yantara, S. A. Veldhuis, L. Martínez-Sarti, B. Chandran, V. Chirvony, A. S. Z. Lo, J. So, C. Soci, M. Grätzel, H. J. Bolink, N. Mathews and S. G. Mhaisalkar, *Energy Environ. Sci.*, 2018, **11**, 1770–1778.

14 O. Chen, J. Zhao, V. P. Chauhan, J. Cui, C. Wong, D. K. Harris, H. Wei, H. S. Han, D. Fukumura, R. K. Jain and M. G. Bawendi, *Nat. Mater.*, 2013, **12**, 445–451.

15 J. Song, J. Li, X. Li, L. Xu, Y. Dong and H. Zeng, *Adv. Mater.*, 2015, **27**, 7162–7167.

16 M. Kulbak, S. Gupta, N. Kedem, I. Levine, T. Bendikov, G. Hodes and D. Cahen, *J. Phys. Chem. Lett.*, 2016, **7**, 167–172.

17 L. Protesescu, S. Yakunin, M. I. Bodnarchuk, A. Walsh, F. Krieg, R. Caputo, C. H. Hendon, R. X. Yang and M. V. Kovalenko, *Nano Lett.*, 2015, **15**, 3692–3696.

18 J. De Roo, M. Ibáñez, P. Geiregat, G. Nedelcu, I. Van Driessche, Z. Hens, W. Walravens, J. C. Martins, J. Maes and M. V. Kovalenko, *ACS Nano*, 2016, **10**, 2071–2081.

19 Y. Tan, Y. Zou, L. Wu, Q. Huang, D. Yang, M. Chen, M. Ban, C. Wu, T. Wu, S. Bai, T. Song, Q. Zhang and B. Sun, *ACS Appl. Mater. Interfaces*, 2018, **10**, 3784–3792.

20 D. P. Nenon, K. Pressler, W. T. Osowiecki, J. H. Olshansky, A. P. Alivisatos, L.-W. Wang, J. Kang, B. A. Koscher and M. A. Koc, *J. Am. Chem. Soc.*, 2018, **140**, 17760–17772.

21 Q. A. Akkerman, L. Manna, H. J. Snaith, I. Infante, U. Petralanda, L. Goldoni, D. Maggioni, O. J. Ashton, G. Almeida and N. Mishra, *J. Am. Chem. Soc.*, 2018, **140**, 14878–14886.

22 T. Wang, L. Xu, J. Chen, J. Li, J. Song, B. Han, H. Zeng, Q. Shan, Y. Dong, B. Cai and J. Xue, *Adv. Mater.*, 2016, **29**, 1603885.

23 J. Maes, L. Balcaen, E. Drijvers, Q. Zhao, J. De Roo, A. Vantomme, F. Vanhaecke, P. Geiregat and Z. Hens, *J. Phys. Chem. Lett.*, 2018, **9**, 3093–3097.

24 A. Teitelboim, L. Avram, M. Menahem, M. Kazes, T. Wolf, T. Udayabhaskararao, O. Yaffe, I. Pinkas, M. Leskes,

D. Oron, H. Cohen and L. Houben, *Chem. Mater.*, 2017, **30**, 84–93.
25 S. K. Davidowski and G. P. Holland, *Langmuir*, 2016, **32**, 3253–3261.
26 M. Tassi, D. Geldof, A. Roevens, F. Blockhuys, R. Carleer, P. Adriaensens and V. Meynen, *Surf. Sci.*, 2016, **655**, 31–38.
27 G. P. Holland, R. Sharma, J. O. Agola, S. Amin, V. C. Solomon, P. Singh, D. A. Buttry and J. L. Yarger, *Chem. Mater.*, 2007, **19**, 2519–2526.
28 R. Gomes, A. Hassinen, A. Szczygiel, Q. Zhao, A. Vantomme, J. C. Martins and Z. Hens, *J. Phys. Chem. Lett.*, 2011, **2**, 145–152.
29 A. P. Alivisatos, J. S. Owen, J. Park and P.-E. Trudeau, *J. Am. Chem. Soc.*, 2008, **130**, 12279–12281.
30 K. De Keukeleere, S. Coucke, E. De Canck, P. Van Der Voort, F. Delpech, Y. Coppel, Z. Hens, I. Van Driessche, J. S. Owen and J. De Roo, *Chem. Mater.*, 2017, **29**, 10233–10242.
31 M. I. Bodnarchuk, S. C. Boehme, S. Ten Brinck, C. Bernasconi, Y. Shynkarenko, F. Krieg, R. Widmer, B. Aeschlimann, D. Günther, M. V. Kovalenko and I. Infante, *ACS Energy Lett.*, 2019, **4**, 63–74.
32 L. Manna, L. W. Wang, R. Cingolani and A. P. Alivisatos, *J. Phys. Chem. B*, 2005, **109**, 6183–6192.
33 S. R. Smock, T. J. Williams and R. L. Brutchey, *Angew. Chem., Int. Ed.*, 2018, **90089**, 11711–11715.
34 J. W. Blanchard, T. L. Groy, J. L. Yarger and G. P. Holland, *J. Phys. Chem. C*, 2012, **116**, 18824–18830.
35 G. P. Holland, R. Sharma, J. O. Agola, S. Amin, V. C. Solomon, P. Singh, D. A. Buttry and J. L. Yarger, *Chem. Mater.*, 2007, **19**, 2519–2526.
36 J. Y. Woo, S. Lee, S. Lee, W. D. Kim, K. Lee, K. Kim, H. J. An, D. C. Lee and S. Jeong, *J. Am. Chem. Soc.*, 2016, **138**, 876–883.
37 P. Cottingham and R. L. Brutchey, *Chem. Commun.*, 2016, **52**, 5246–5249.
38 F. Brodard-Severac, G. Guerrero, J. Maquet, P. Florian, C. Gervais and P. H. Mutin, *Chem. Mater.*, 2008, **20**, 5191–5196.
39 X. Li, M. Ibrahim Dar, C. Yi, J. Luo, M. Tschumi, S. M. Zakeeruddin, M. K. Nazeeruddin, H. Han and M. Grätzel, *Nat. Chem.*, 2015, **7**, 703–711.
40 I. O. Perez De Berti, M. V. Cagnoli, G. Pecchi, J. L. Alessandrini, S. J. Stewart, J. F. Bengoa and S. G. Marchetti, *Nanotechnology*, 2013, **24**, 1–11.